Observable-specific phase biases of Wuhan multi-GNSS experiment analysis center's rapid satellite products

Jianghui Geng[1,2], Qiyuan Zhang[1], Guangcai Li[1*] ⓘ, Jingnan Liu[1] and Donglie Liu[3*]

Abstract

Precise Point Positioning (PPP) with Ambiguity Resolution (AR) is an important high-precision positioning technique that is gaining popularity in geodetic and geophysical applications. The implementation of PPP-AR requires precise products such as orbits, clocks, code, and phase biases. As one of the analysis centers of the International Global Navigation Satellite System (GNSS) Service (IGS), the Wuhan University Multi-GNSS experiment (WUM) Analysis Center (AC) has provided multi-GNSS Observable-Specific Bias (OSB) products with the associated orbit and clock products. In this article, we first introduce the models and generation strategies of WUM rapid phase clock/bias products and orbit-related products (with a latency of less than 16 h). Then, we assess the performance of these products by comparing them with those of other ACs and by testing the PPP-AR positioning precision, using data from Day of the Year (DOY) 047 to DOY 078 in 2022. It is found that the peak-to-peak value of phase OSBs is within 2 ns, and their fluctuations are caused by the clock day boundary discontinuities. The associated Global Positioning System (GPS) orbits have the best consistency with European Space Agency (ESA) products, and those of other systems rank in the medium place. GLObal NAvigation Satellite System (GLONASS) clocks show slightly inconsistency with other ACs' due to the antenna thrust power adopted, while the phase clocks of other GNSSs show no distortion compared with legacy clocks. With well-estimated phase products for Precise Orbit Determination (POD), the intrinsic precision is improved by 14%, 17%, and 24% for GPS, Galileo navigation satellite system (Galileo), and BeiDou-3 Navigation Satellite System (BDS-3), respectively. The root mean square of PPP-AR using our products in static mode with respect to IGS weekly solutions can reach 0.16 cm, 0.16 cm, and 0.44 cm in the east, north, and up directions, respectively. The multi-GNSS wide-lane ambiguity fixing rates are all above 90%, while the narrow-lane fixing rates above 80%. In conclusion, the phase OSB products at WUM have good precision and performance, which will benefit multi-GNSS PPP-AR and POD.

Keywords: Multi global navigation satellite system, Observable-specific phase bias, Precise point positioning with ambiguity resolution, Wuhan University multi-GNSS experiment analysis center, Precise orbit determination

Introduction

Precise Point Positioning with Ambiguity Resolution (PPP-AR) can achieve millimeter-level accuracy for daily static positioning and centimeter-level accuracy for kinematic positioning. (e.g., Ge et al., 2008; Geng et al., 2019a among others). Although no differencing of the simultaneously tracked measurements from multiple receivers is required, the implementation of PPP-AR requires precise products such as orbits, clocks, code, and phase biases. Such products are regularly generated by the

*Correspondence: guangcai.li@whu.edu.cn; donglie.liu@westernbeidou.com

[1] GNSS Research Center, Wuhan University, 129 Luoyu Road, Wuhan 430079, China

[3] Natural Resources Satellite Remote Sensing Application Center, 242 Zhonghuabei Road, Guiyang 550004, China

Full list of author information is available at the end of the article

Analysis Centers (ACs) of the nternational GNSS (Global Navigation Satellite System) Service (IGS) by processing the observations from a global network of GNSS stations (Beutler et al., 2009). In the early stage, the basic core products included orbits, clocks, and earth rotation parameters of Global Positioning System (GPS) and GLObal NAvigation Satellite System (GLONASS). With the development of multi-GNSS, the IGS Multi-GNSS Working Group initiated the Multi-GNSS EXperiment (MGEX) in 2012, aiming at the generation of multi-GNSS precise products including GPS, GLONASS, Galileo navigation satellite system (Galileo), BeiDou Navigation Satellite System (BDS), and Quasi-Zenith Satellite System (QZSS) (Montenbruck et al., 2014).

Unlike the established satellite orbit and clock products, phase bias products for PPP-AR have only been released by the IGS in recent years (e.g., Banville et al., 2020; Schaer et al., 2021). However, these phase bias products are crucial in PPP-AR because they are necessary to recover the integer property of ambiguities. Nominal phase biases are hardware biases of the receiver and the satellite, which are highly correlated with the satellite clock offset and ambiguity parameters in the least-squares estimator. Hence, these biases are usually extracted from ambiguities in a network solution, with the fact that hardware delays from one transmitter are identical across the network (Ge et al., 2008).

Some well-known phase bias models are used for PPP-AR, including the Uncalibrated Phase Delay (UPD) model (Ge et al., 2008), the integer clock model (Laurichesse et al., 2009), and the decoupled clock model (Collins et al., 2010). These models are implemented by different IGS ACs. To be specific, the European Space Agency (ESA) implemented the ambiguity-fixed UPD model to provide PPP users with both wide- and narrow-lane UPD products, along with IGS legacy satellite clocks (Banville et al., 2020). The Centre National d'Etudes Spatiales (CNES) employed the integer clock model to provide both wide-lane UPDs and re-estimated clocks merged with ionosphere-free UPDs (Laurichesse et al., 2009). Further, the Natural Resources Canada (NRCan or EMR) adopted the decoupled clock model, which is a modified approach to the integer clock model, and provided a phase-datum integer clock containing the time-varying phase biases (Collins et al., 2010). WuHan University (WHU) employed the phase clock/bias model, which is mathematically equivalent to the integer clock model while maintaining compatibility with IGS legacy clocks (Geng et al., 2019b). Besides, the Center for Orbit Determination in Europe (CODE) adopted the common clock model, providing daily observable-specific signal bias per satellite (Schaer et al., 2021). Graz University of Technology (TUG) used multi-frequency raw observations

in data processing, with signal-specific phase biases as unknowns (Strasser et al., 2019).

In 2018, a PPP-AR working group was established within the framework of IGS, boosting the generation of phase products in standard format (Schaer 2016a). To ensure the interoperability of bias products from ACs, the Observable-specific Signal Biases (OSBs) framework, instead of Differential Code Bias (DCB) or UPDs, is preferred by the IGS. In the OSB framework, bias products should contain the corrections for each channel of code and phase signals, and users only need to subtract the individual bias from the raw observation. Schaer (2016b) released standard code OSB format Bias- Solution INdependent EXchange format (SINEX) 1.0, and many ACs have provided code bias products in the OSB framework (e.g., CODE, GFZ, etc.). Schaer et al. (2021) further proposed that phase bias can also be unified in Bias-SINEX 1.0 format. The OSB framework has good interoperability such that the phase biases from different AR methods can be accommodated. So far, most ACs have provided only dual-frequency phase OSBs, since the data processing is based on the ionosphere-free combination. An extension to multi-frequencies is still under investigation, but promisingly, methods have been developed to access the multi-frequency phase OSBs (Geng et al., 2022; Laurichesse, 2015).

In the OSB framework, we provide the observable-specific phase bias products of Wuhan University, which can be freely downloaded at ftp://igs.gnsswhu.cn/pub/whu/phasebias/. To be specific, we first released the phase products in 2019 with the COD final orbits fixed, and only GPS clock and bias products (Geng et al., 2019a, 2019b). In 2020, we released the multi-GNSS phase bias products including GPS, Galileo, BDS, and QZSS, and the orbits were WUM final orbits (Guo et al., 2016). According to Banville et al. (2020), the WUM phase bias products have already delivered an excellent PPP-AR result. However, the time latency of WUM final products is more than one week, which is not in time for the research in earthquake or deformation monitoring. Besides, the clock along with phase bias is correlated with orbit parameters in the least-square estimator, hence there are inconsistencies if the products are based on different software and observation network. To address these two issues, our efforts are to reduce time latency and promote product interoperability. We follow the requirement of IGS Rapid, providing multi-GNSS products including orbit, earth rotation parameters, and attitude quaternions with latency no longer than 16 h.

The goal of this paper is to introduce the WUM rapid products for the potential users of our products. We described the models and generation strategies of these products and assessed their performance by comparing

them with those of other ACs and by testing the PPP-AR positioning precision, using the data from Day of Year (DOY) 047 to DOY 078 in 2022. Moreover, the impact on satellite orbit precision with between-satellite Single-Difference (SD) or double-difference ambiguity resolution is discussed. It is worthy to mention that the ambiguity resolution can only be achieved in double-difference mode. The between-satellite single-difference ambiguities need no differencing between receivers, but single-difference phase biases instead to be resolved, which makes up the double-difference mode. However, we distinguish the two combinations of ambiguities, i.e., the double-difference ambiguities, the ambiguities differenced twice between satellites and receivers, and the single-difference ambiguities, the ambiguities differenced once between satellites. We found that the between-satellite single-difference ambiguity resolution achieved better orbit precision than the double-difference ambiguity resolution. This study is organized as follows: Section "Method" introduces how the modified phase/clock model is implemented in the WUM product generation; "Generation of satellite phase clock/bias and orbit product" section describes the daily processing model of all precise products; "Data and experiments" section shows the experimental setup and the data; "Results" section portrays the detailed evaluation results; "Discussion" section discusses the orbit precision with the between-satellite single-difference AR against the double-difference AR. The conclusions are drawn in "Conclusion" section.

Method

Generation of satellite phase clock/bias and orbit product

Raw GPS/Galileo/BDS dual-frequency pseudorange and carrier-phase observations between receiver i and satellite j in the unit of length can be expressed as

$$
\begin{cases}
P_{i,1}^j = \rho_i^j + c(t_i - t^j) + T_i^j + \dfrac{I_i^j}{f_1^2} + b_{i,1} - b_1^j + \varepsilon_{i,1}^j \\[2mm]
P_{i,2}^j = \rho_i^j + c(t_i - t^j) + T_i^j + \dfrac{I_i^j}{f_2^2} + b_{i,2} - b_2^j + \varepsilon_{i,2}^j \\[2mm]
L_{i,1}^j = \rho_i^j + c(t_i - t^j) + T_i^j - \dfrac{I_i^j}{f_1^2} + \lambda_1 N_{i,1}^j + B_{i,1} - B_1^j + \xi_{i,1}^j \\[2mm]
L_{i,2}^j = \rho_i^j + c(t_i - t^j) + T_i^j - \dfrac{I_i^j}{f_2^2} + \lambda_2 N_{i,2}^j + B_{i,2} - B_2^j + \xi_{i,2}^j
\end{cases}
\tag{1}
$$

where $P_{i,1}^j$ and $P_{i,2}^j$ represent pseudorange observations, whereas $L_{i,1}^j$ and $L_{i,2}^j$ are carrier-phase observations on frequencies f_1 and f_2; ρ_i^j denotes the geometric distance between the receiver i and the satellite j; c is the speed of light in vacuum; t_i and t^j are the receiver and satellite clock offsets; T_i^j is the tropospheric delay and I_i^j is the first-order ionosphere delay. λ_1 and λ_2 are wavelengths of

frequencies f_1 and f_2; $b_{i,1}$ and $b_{i,2}$ denote the pseudorange hardware biases for the receiver i, whereas b_1^j and b_2^j are for the satellite j; $B_{i,1}$ and $B_{i,2}$ are the carrier-phase hardware biases in the unit of cycle for the station i, while B_1^j and B_2^j are for the satellite j; $N_{i,1}^j$ and $N_{i,2}^j$ are integer ambiguities; $\varepsilon_{i,1}^j$ and $\varepsilon_{i,2}^j$ are pseudorange noise, whereas $\xi_{i,1}^j$ and $\xi_{i,2}^j$ are carrier-phase noise.

To eliminate ionosphere delay, ionosphere-free pseudorange and carrier-phase observations can be written as

$$
\begin{cases}
P_{i,\mathrm{IF}}^j = \alpha P_{i,1}^j - \beta P_{i,2}^j \\
\quad = \rho_i^j + c(t_i - t^j) + T_i^j + b_{i,\mathrm{IF}} - b_{\mathrm{IF}}^j + \varepsilon_i^j \\
L_{i,\mathrm{IF}}^j = \alpha L_{i,1}^j - \beta L_{i,2}^j \\
\quad = \rho_i^j + c(t_i - t^j) + T_i^j + \lambda_1 N_{i,\mathrm{IF}}^j + B_{i,\mathrm{IF}} - B_{\mathrm{IF}}^j + \xi_i^j
\end{cases}
\tag{2}
$$

and

$$
\begin{cases}
B_{i,\mathrm{IF}} = \alpha B_{i,1} - \beta B_{i,2} \\
B_{\mathrm{IF}}^j = \alpha B_1^j - \beta B_2^j \\
b_{i,\mathrm{IF}} = \alpha b_{i,1} - \beta b_{i,2} \\
b_{\mathrm{IF}}^j = \alpha b_1^j - \beta b_2^j \\
\lambda_1 N_{i,\mathrm{IF}}^j = \lambda_w \lambda_n N_{i,w}^j / \lambda_2 + \lambda_n N_{i,n}^j
\end{cases}
\tag{3}
$$

where $\alpha = \dfrac{f_1^2}{f_1^2 - f_2^2}$ and $\beta = \dfrac{f_2^2}{f_1^2 - f_2^2}$ are coefficients of the ionosphere-free combination; $P_{i,\mathrm{IF}}^j$ and $L_{i,\mathrm{IF}}^j$ are ionosphere-free pseudorange and carrier-phase observables, respectively. $\lambda_w = \dfrac{c}{f_1 - f_2}$ and $\lambda_n = \dfrac{c}{f_1 + f_2}$ are regarded as the wide-lane and narrow-lane wavelengths. $N_{i,w}^j = N_{i,1}^j - N_{i,2}^j$ and $N_{i,n}^j = N_{i,1}^j$ are wide-lane and narrow-lane ambiguities.

From Eq. (3), we can see that ionosphere-free ambiguity resolution can be achieved by resolving wide-lane and narrow-lane ambiguities. For wide-lane ambiguity resolution, the Melbourne-Wübbena (MW) combination measurement is constituted as

$$
\begin{aligned}
L_{i,\mathrm{MW}}^j &= \frac{1}{f_1 - f_2}(f_1 L_{i,1}^j - f_2 L_{i,2}^j) - \frac{1}{f_1 + f_2}(f_1 P_{i,1}^j - f_2 P_{i,2}^j) \\
&= \lambda_w(N_{i,w}^j + b_{i,w}^j) + \varepsilon \\
b_{i,w}^j &= \left(\frac{B_{i,1} - B_1^j}{\lambda_1} - \frac{B_{i,2} - B_2^j}{\lambda_2} \right) \\
&\quad - \frac{\lambda_n}{\lambda_w}\left(\frac{b_{i,1} - b_1^j}{\lambda_1} - \frac{b_{i,2} - b_2^j}{\lambda_2} \right)
\end{aligned}
\tag{4}
$$

where $b_{i,w}^j$ denotes the bias term of wide-lane ambiguity $N_{i,w}^j$. Since its integer component can be absorbed by

$N_{i,w}^{j}$, here it only represents its fractional part, which is called wide-lane UPD or wide-lane Fractional-Cycle Bias (FCB). After excluding the bias term $b_{i,w}^{j}$, the wide-lane ambiguity $N_{i,w}^{j}$ can be fixed.

After a least-square estimation, hardware biases will be assimilated into satellite clocks, receiver clocks, ambiguities, and observation residuals (Ge et al., 2008). We thus reformulate Eq. (2) as

$$
\begin{cases}
P_{i,\mathrm{IF}}^{j} = \rho_i^j + c\left(t_i + \dfrac{b_{i,\mathrm{IF}}}{c} - \left(t^j + \dfrac{b_{\mathrm{IF}}^j}{c}\right)\right) + T_i^j + \varepsilon_i^j \\[2mm]
L_{i,\mathrm{IF}}^{j} = \rho_i^j + c\left(t_i + \dfrac{b_{i,\mathrm{IF}}}{c} - \left(t^j + \dfrac{b_{\mathrm{IF}}^j}{c}\right)\right) + T_i^j \\[2mm]
\qquad\quad + \lambda_1\left(N_{i,\mathrm{IF}}^{j} + \dfrac{B_{i,\mathrm{IF}} - B_{\mathrm{IF}}^{j} - b_{i,\mathrm{IF}} + b_{\mathrm{IF}}^{j}}{\lambda_1}\right) + \xi_i^j
\end{cases}
\tag{5}
$$

where $N_{i,\mathrm{IF}}^{j} + \dfrac{B_{i,\mathrm{IF}} - B_{\mathrm{IF}}^{j} - b_{i,\mathrm{IF}} + b_{\mathrm{IF}}^{j}}{\lambda_1}$ is the ambiguity to be resolved; $t^j + \dfrac{b_{\mathrm{IF}}^{j}}{c}$ is the theoretical expression of the IGS legacy clocks. The fraction component of the ionosphere-free ambiguity is the ionosphere-free UPD, referred to as the narrow-lane UPD in this article.

The phase clock/bias model
Geng et al. (2019b) mentioned that hardware biases could be divided into two parts, the time-invariable portions are assimilated into ambiguities, whereas the time-variable portions are absorbed by clock parameters. Therefore, the hardware biases in Eq. (2) can be rewritten as

$$
\begin{cases}
b_{i,\mathrm{IF}} = \Delta b_{i,\mathrm{IF}} + \delta b_{i,\mathrm{IF}} \\[1mm]
b_{\mathrm{IF}}^{j} = \Delta b_{\mathrm{IF}}^{j} + \delta b_{\mathrm{IF}}^{j} \\[1mm]
B_{i,\mathrm{IF}} = \Delta B_{i,\mathrm{IF}} + \delta B_{i,\mathrm{IF}} \\[1mm]
B_{\mathrm{IF}}^{j} = \Delta B_{\mathrm{IF}}^{j} + \delta B_{\mathrm{IF}}^{j}
\end{cases}
\tag{6}
$$

where $\Delta b_{i,\mathrm{IF}}, \Delta b_{\mathrm{IF}}^{j}, \Delta B_{i,\mathrm{IF}}, \Delta B_{\mathrm{IF}}^{j}$ are constant portions and $\delta b_{i,\mathrm{IF}}, \delta b_{i,\mathrm{IF}}, \delta B_{i,\mathrm{IF}}, \delta B_{\mathrm{IF}}^{j}$ are time-variable portions.

Correspondingly, Eq. (5) can be reformulated as

$$
\begin{cases}
P_{i,\mathrm{IF}}^{j} = \rho_i^j + c\left(t_i + \dfrac{\Delta b_{i,\mathrm{IF}} + \delta B_{i,\mathrm{IF}}}{c} - \left(t^j + \dfrac{\Delta b_{\mathrm{IF}}^j + \delta B_{\mathrm{IF}}^j}{c}\right)\right) + T_i^j \\[2mm]
\qquad\quad + (\delta b_{i,\mathrm{IF}} - \delta b_{\mathrm{IF}}^{j} - \delta B_{i,\mathrm{IF}} + \delta B_{\mathrm{IF}}^{j}) + \varepsilon_i^j \\[2mm]
L_{i,\mathrm{IF}}^{j} = \rho_i^j + c\left(t_i + \dfrac{\Delta b_{i,\mathrm{IF}} + \delta B_{i,\mathrm{IF}}}{c} - \left(t^j + \dfrac{\Delta b_{\mathrm{IF}}^j + \delta B_{\mathrm{IF}}^j}{c}\right)\right) + T_i^j \\[2mm]
\qquad\quad + \lambda_1\left(N_{i,\mathrm{IF}}^{j} + \dfrac{\Delta B_{i,\mathrm{IF}} - \Delta B_{\mathrm{IF}}^{j} - \Delta b_{i,\mathrm{IF}} + \Delta b_{\mathrm{IF}}^{j}}{\lambda_1}\right) + \xi_i^j
\end{cases}
\tag{7}
$$

with Eq. (3)

$$
\begin{cases}
P_{i,\mathrm{IF}}^{j} = \rho_i^j + c\left(t_i + \dfrac{\Delta b_{i,\mathrm{IF}} + \delta B_{i,\mathrm{IF}}}{c} - \left(t^j + \dfrac{\Delta b_{\mathrm{IF}}^j + \delta B_{\mathrm{IF}}^j}{c}\right)\right) + T_i^j \\[2mm]
\qquad\quad + (\delta b_{i,\mathrm{IF}} - \delta b_{\mathrm{IF}}^{j} - \delta B_{i,\mathrm{IF}} + \delta B_{\mathrm{IF}}^{j}) + \varepsilon_i^j \\[2mm]
L_{i,\mathrm{IF}}^{j} = \rho_i^j + c(t_i + \dfrac{\Delta b_{i,\mathrm{IF}} + \delta B_{i,\mathrm{IF}}}{c} - (t^j + \dfrac{\Delta b_{\mathrm{IF}}^j + \delta B_{\mathrm{IF}}^j}{c})) + T_i^j \\[2mm]
\qquad\quad + \lambda_n\dfrac{\lambda_w}{\lambda_2}N_{i,w}^{j} - \lambda_n(N_{i,n}^{j} - \dfrac{\Delta B_{i,\mathrm{IF}} - \Delta B_{\mathrm{IF}}^{j} - \Delta b_{i,\mathrm{IF}} + \Delta b_{\mathrm{IF}}^{j}}{\lambda_n}) + \xi_i^j
\end{cases}
\tag{8}
$$

where $\dfrac{\Delta B_{i,\mathrm{IF}} - \Delta B_{\mathrm{IF}}^{j} - \Delta b_{i,\mathrm{IF}} + \Delta b_{\mathrm{IF}}^{j}}{\lambda_n}$ becomes the bias term of the narrow-lane ambiguity $N_{i,n}^{j}$, and its fractional part is called the narrow-lane UPD.

From Eqs. (4) and (8), the implementation of wide-lane and narrow-lane ambiguity resolution requires beforehand bias corrections, *i.e.*, wide-lane and narrow-lane UPDs. These UPD products are estimated in a network solution (Ge et al., 2008). In the network solution, wide-lane UPDs are computed using the MW observables (Eq. (4)). To remove station-dependent biases, single differencing between satellites is carried out on the ambiguity estimates. As a result, the receiver hardware delays are eliminated, and the remaining UPDs are only satellite-dependent and identical across stations within the network. Therefore, the single-difference wide-lane UPD for the satellite pair j and k is

$$D_w^{j,k} = \frac{1}{S^{j,k}} \sum_{i=1}^{S^{j,k}} (L_{i,\mathrm{MW}}^{j,k} - [L_{i,\mathrm{MW}}^{j,k}]) \tag{9}$$

where $D_w^{j,k}$ denotes the single-difference UPD for the satellite pair j and k, and $S^{j,k}$ is the number of single-difference MW observables from all reference stations; [] represents an operation of rounding to the nearest integer; $L_{i,\mathrm{MW}}^{j,k}$ is the difference of $L_{i,\mathrm{MW}}^{j}$ and $L_{i,\mathrm{MW}}^{k}$. In consideration of the stability of the wide-lane UPD, the wide-lane UPDs are generated every 24 h.

Once the wide-lane UPDs are extracted, the integer wide-lane ambiguities can be separated from MW observations. Similar to Eq. (9), we can use the integer wide-lane ambiguity to obtain the real-valued estimate of the narrow-lane ambiguity $\hat{N}_{n,i}^{j,k}$. However, unlike the double-difference AR, this narrow-lane ambiguity is affected by the bias term, i.e., narrow-lane UPD. The narrow-lane UPD estimate for the satellite pair j and k can be obtained with

$$D_n^{j,k} = \frac{1}{S^{j,k}} \sum_{i=1}^{S^{j,k}} (\hat{N}_{n,i}^{j,k} - [\hat{N}_{n,i}^{j,k}]) \tag{10}$$

where $D_n^{j,k}$ is the single-difference narrow-lane UPD. Due to orbit errors, clock errors, and residual troposphere delays, the narrow-lane UPDs are not stable over time. Hence, Ge et al. (2008) recommended that narrow-lane UPDs should be estimated every 15 min. Once the narrow-lane UPDs are obtained, we can use them to resolve the integer narrow-lane ambiguity $\breve{N}_{i,n}^{j,k}$ at each station:

$$\breve{N}_{i,n}^{j,k} = [\hat{N}_{i,n}^{j,k} - D_n^{j,k}] \tag{11}$$

However, as shown in Eq. (7), the time-variable portion of hardware delays can be assimilated into the satellite clocks, while the remaining time-invariable portion can be reserved as the stable UPD products. Therefore, Geng et al. (2019b) further used these 15-min narrow-lane UPDs

to obtain daily mean narrow-lane UPDs to constrain the nominal ionosphere-free ambiguity,

$$\begin{cases} \lambda_1 N_{i,\mathrm{IF}}^{j,k} - \Delta B_{\mathrm{IF}}^{j,k} + \Delta b_{\mathrm{IF}}^{j,k} = \lambda_w \lambda_n \breve{N}_{i,w}^{j,k}/\lambda_2 - \lambda_n (\breve{N}_{i,n}^{j,k} + \overline{D}_n^{j,k}) \\ \overline{D}_n^{j,k} = \frac{1}{S_n^{j,k}} \sum_{i=1}^{S_n^{j,k}} D_{n,i}^{j,k} \end{cases} \tag{12}$$

where $\overline{D}_n^{j,k}$ denotes daily narrow-lane UPDs, and $S_n^{j,k}$ is the number of 15-min narrow-lane UPDs; $\breve{N}_{i,w}^{j,k}$ is the resolved integer wide-lane ambiguity like Eq. (10). The single-difference UPDs can be transformed into undifferenced UPD for each satellite by adding a pivot UPD, but they are sufficient for the between-satellite single-difference ambiguity resolution. The resolved ambiguity will be introduced in the normal matrix and constraints the estimation of undifferenced ambiguity. The corresponding Eq. (12) is substituted into Eq. (8) to re-estimate the satellite clock

$$\bar{t}^j = t^j + \frac{\Delta b_{\mathrm{IF}}^j + \delta B_{\mathrm{IF}}^j}{c} \tag{13}$$

where $\bar{t}^j$ is called the satellite phase clock. As a result, to implement GNSS precise orbit determination based on the between-satellite single-difference ambiguity resolution using this phase clock/bias model, the satellite phase clocks as well as the daily wide-lane and narrow-lane UPD products will be used.
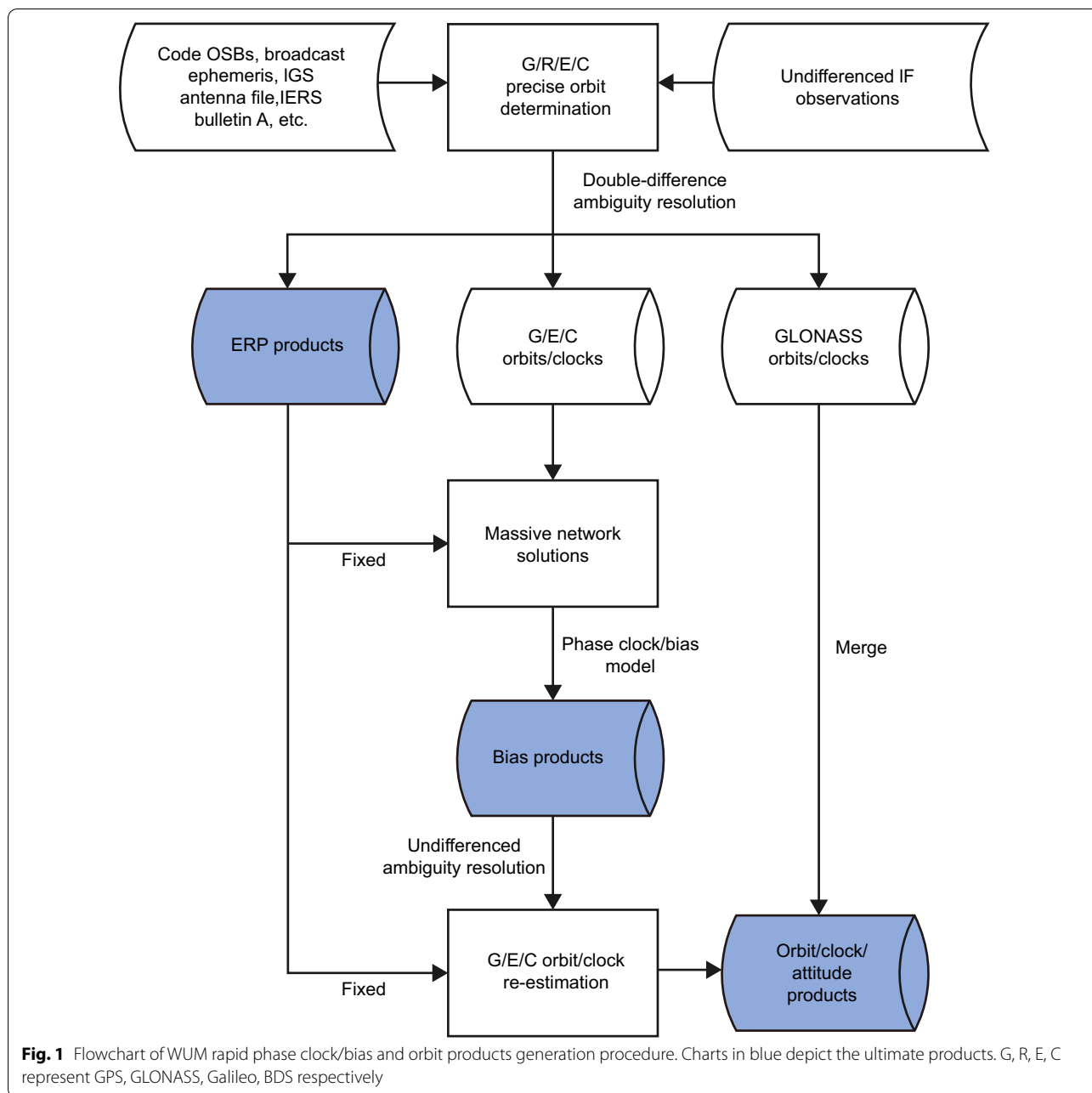
In addition, wide-lane and narrow-lane UPDs can be converted to phase observable-specific biases with

$$\begin{pmatrix} B_1^j \\ B_2^j \\ d_1^j \\ d_2^j \end{pmatrix} = \begin{pmatrix} \frac{f_1}{f_1-f_2} & \frac{-f_2}{f_1-f_2} & \frac{-f_1}{f_1+f_2} & \frac{-f_2}{f_1+f_2} \\ \alpha & \beta & 0 & 0 \\ 0 & 0 & 1 & -1 \\ 0 & 0 & \alpha & \beta \end{pmatrix}^{-1} \begin{pmatrix} \lambda_w D_w^j \\ \lambda_n \overline{D}_n^j \\ D_{\mathrm{P1P2}} \\ 0 \end{pmatrix} \tag{14}$$

where B_1^j and B_2^j are phase observable-specific biases of the satellite j for f_1 and f_2, respectively; d_1^j and d_2^j are the corresponding code biases, and their ionosphere-free combination was constrained to zero to eliminate the rank deficiency caused by the linear dependence between different types of code OSBs from each satellite, as described in Liu et al. (2021); and B_{P1P2} is the differential code bias between P1 and P2 in meters.

Generation of satellite phase clock/bias and orbit product
Processing procedure
Figure 1 shows the procedure to derive WUM GNSS bias products using the phase clock/bias model. There are three steps as follows.

Fig. 1 Flowchart of WUM rapid phase clock/bias and orbit products generation procedure. Charts in blue depict the ultimate products. G, R, E, C represent GPS, GLONASS, Galileo, BDS respectively

First, orbits and clocks are calculated with about 150 IGS network stations. We first estimate GPS/GLONASS/Galileo orbits and clocks and estimate BDS orbits and clocks while holding the GPS products fixed. The undifferenced ambiguities from simultaneously monitoring stations are combined as double-difference ambiguities, which are fixed and constrained in the estimation to improve the orbit precision. After this step, precise orbits, Earth Rotation Parameter (ERP), and clocks are derived. Meanwhile, clock densification is implemented

to transform 300-s clocks into 30-s clock products (Chen et al., 2014).

Second, the phase OSB products are estimated. PPP processing is conducted within a larger network containing over 200 stations. The ambiguities from the whole network are gathered to compute phase OSBs, according to Eqs. (9–14). In this step, GPS, Galileo, and BDS ambiguities are estimated together. Considering the orbit precision of Galileo and the imperfect error models like BDS Phase Center Offsets (PCOs), we down-weight

Geng *et al. Satellite Navigation*   (2022) 3:23

Page 7 of 15

Table 1 Data processing models and strategies

Items	Strategies
Observations	Undifferenced ionosphere-free combination of GPS L1/L2, Galileo E1/E5a, BDS B1I/B3I observations
Observation noise	Pseudorange: 0.5 m; Carrier-phase: 0.01 cycles
PCO/PCV	igs14.atx for satellites and stations
Tropospheric delay	Global Pressure and Temperature (GPT) model with Global Mapping Function (GMF), hourly Zenith Total Delay (ZTD), and 24-h gradients (Boehm et al., 2007)
Earth rotation	Universal Time (UT1) is fixed; x- and y-pole coordinates, dx, dy, and Length Of Day (LOD) are estimated
Tidal displacement	International Earth Rotation Service (IERS) Conventions 2010, global tide Finite Element Solution 2014b (FES2014b) for ocean tides (Spiridonov and Vinogradova 2020)
Relativity effect	IERS Conventions 2010
Earth gravity	Earth Gravitational Model 2008 (EGM08) 12°
Perturbations	Sun, Moon, and planets in JPL Development Ephemeris 405 (DE405)
Solar radiation	ECOM1 5-parameters with a priori model for Galileo; ECOM2 9-parameters for GPS without a priori model; ECOM1 5-parameters for BDS-3 IGSO without a priori model; ECOM2 9-parameters for BDS-3 Medium Earth Orbit (MEO) with a priori model (Lou et al., 2014; Springer et al., 1999; Wang et al., 2018a; Yan et al., 2019)
Attitude model	GPS yaw attitude model by Kouba (2009, 2013) and Dilssner (2010); Galileo yaw model with metadata (EGSC, 2017); BDS-3 yaw-steering model (Lin et al., 2018; Wang et al., 2018b; Xia et al., 2019)

the observations of Galileo and BDS by 1/2 and 1/6, respectively.

The final step is updating orbits and clocks using the estimated OSB products. The undifferenced ambiguities are combined as the between-satellite single-difference ambiguities, which are resolved after subtracting phase OSBs. Note that the ERP is not re-estimated in this step because it is not highly correlated with bias products.

The estimated phase OSBs and the adopted code OSBs (Zhang and Zhao, 2020) are merged as the ultimate bias product file. The OSB-updated orbits and clocks are combined with GLONASS counterparts as ultimate orbit and clock products. The 30-s attitude quaternion product is the by-product of orbit integration, and this product can improve clock correction consistency for users (Loyer et al., 2017, 2021). Additionally, we undergo PPP-AR within a test network to check all the products, and the results are compared with the latest IGS weekly coordinate solution. Once the positioning results accord with IGS solutions in normal limits, they will be uploaded to the website of WHU (ftp://igs.gnsswhu.cn/pub/whu/phasebias).
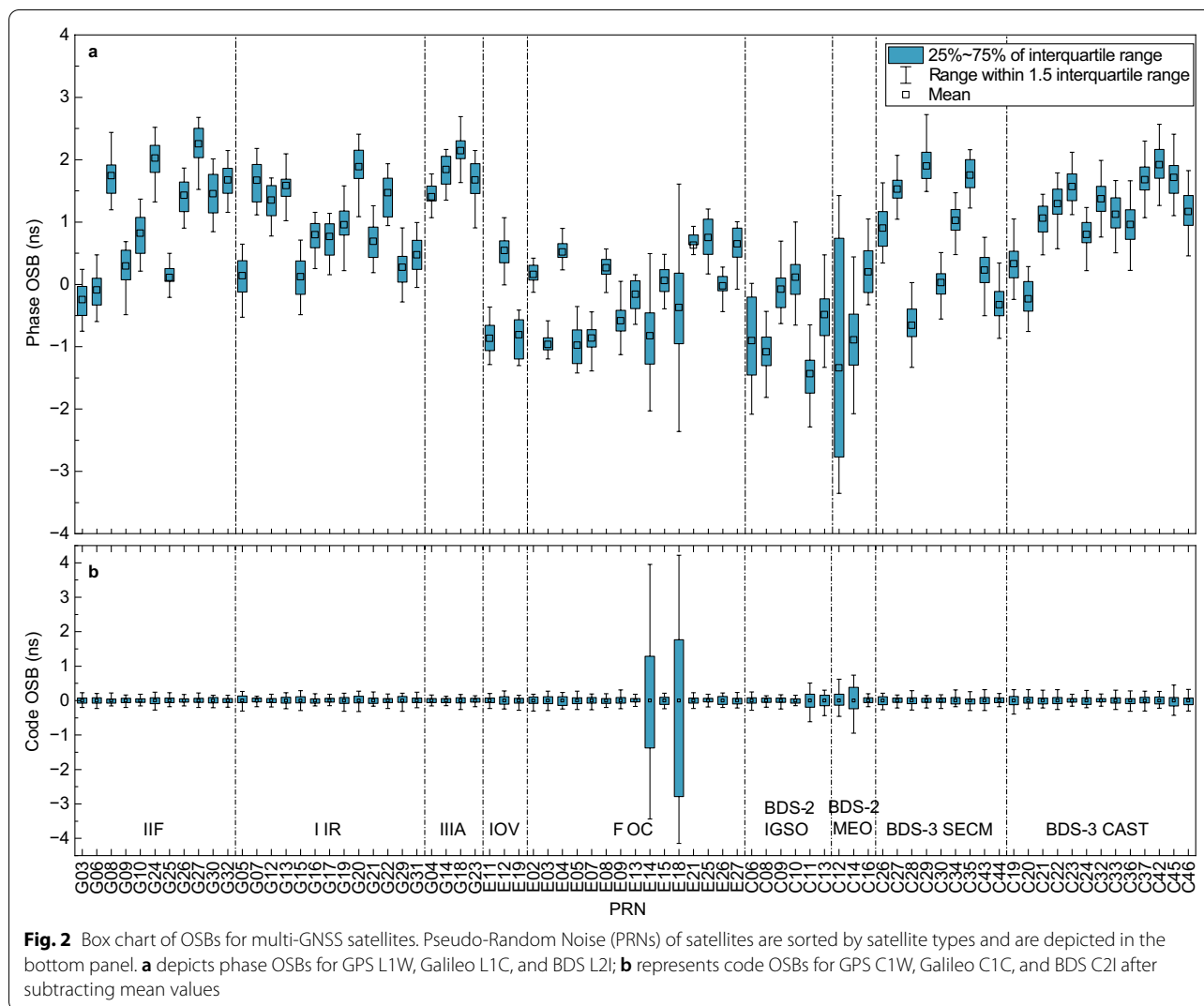
Processing models

Table 1 presents the detailed models and strategies used in the product generation. In the clock estimation, we selected a station equipped with the atomic clock as the datum clock to avoid the rank deficiency caused by receiver and satellite clock parameters. To choose the datum clock of the best quality, we ensured that the picked receiver clock has the lowest STandard Deviation (STD) and no missing epochs. The station coordinates are constrained to the IGS weekly solutions for aligning

Table 2 Full names of included AC

AC ID	Full name
ESA	European space operations centre
COD	Center for orbit determination in Europe
GRG	Groupe de Recherche de Géodésie Spatiale
IAC	Information & analysis center
JAX	Japan aerospace exploration agency
GFZ	Deutsches GeoForschungsZentrum Potsdam
SHA	Shanghai observatory
WHU	Wuhan University

the products with the International Terrestrial Reference Frame (ITRF). Millimeter- or sub-millimeter-level constraints are added to these coordinates according to the accuracy index in the SINEX files.

Inter-System Biases (ISB) are introduced between GNSSs since receiver clocks are aligned to GPS solutions. The ISB parameter is also added between BeiDou-2 Navigation Satellite System (BDS-2) and BDS-3, which can improve positioning precision (Jiao et al., 2019). Inter-Frequency Code Bias parameters (IFCB) are not introduced for GLONASS pseudorange observations since carrier-phase observations are dominant and IFCB estimation is quite time-consuming. Temporarily, the Extended CODE Orbit Model 2 (ECOM-2) 9-parameter model is used for GPS satellites, which will be switched to a 7-parameter model later to be consistent with other ACs. BDS-3 Inclined Geosynchronous Orbit (IGSO) will also adopt the 7-parameter ECOM model since tracking stations are not enough for a 9-parameter ECOM model. For GPS Block IIIA satellites, no maneuver model is

Geng *et al. Satellite Navigation*   (2022) 3:23

Page 8 of 15

Fig. 2 Box chart of OSBs for multi-GNSS satellites. Pseudo-Random Noise (PRNs) of satellites are sorted by satellite types and are depicted in the bottom panel. **a** depicts phase OSBs for GPS L1W, Galileo L1C, and BDS L2I; **b** represents code OSBs for GPS C1W, Galileo C1C, and BDS C2I after subtracting mean values

employed for the time being, and the yaw model of Block IIR will be adopted since they are made by the same manufacturer (Steigenberger et al., 2020).

Data and experiments

The products from DOY 047 to DOY 079 in 2022 are archived for our experiments. To access the quality of our products, we compare our orbit and clock products with archived MGEX products. The involved products include final products from ESA, COD, WHU (WUM), GRG, IAC, and JAX, and rapid products from GFZ (GBM) and SHA. The full names of these ACs are listed in Table 2. In our experiment, we do not distinguish between final products and rapid products, because their precision difference is small and does not affect short-time comparison, and most ACs provide only one kind of MGEX products. Considering that IGS has not combined MGEX

products yet, the products from ESA are chosen as reference, because ESA products are consecutively complete in our experimental spans. ESA also has provided BDS-3 products for years.

To validate our phase OSB products, PPP-AR is conducted with the open-source software PRIDE PPP-AR 2.2 (Geng et al., 2019a). In our experimental timespan, the data from about 200 IGS monitoring stations are gathered each day, and the positioning results are compared with IGS weekly coordinate solutions. The RMS of the coordinate difference after a helmet transformation demonstrates the positioning precision, and the mean fixing rates represent the quality of ambiguity resolution.

Results

GPS/Galileo/BDS phase OSBs

Figure 2 depicts phase OSB and code OSB products for GPS, Galileo, and BDS. In the box chart, a simple

Geng *et al. Satellite Navigation*   (2022) 3:23

Page 9 of 15

distribution is demonstrated by mean value, Inter Quartile Range (IQR), median number, and outliers. The median numbers and outliers are omitted in our plot, and additionally, the mean value is removed for each code OSB series in Fig. 2b. Phase OSBs on L1W for GPS, L2C for Galileo, and L2I for BDS are shown in Fig. 2a. Generally, most of the satellite phase OSBs have peak-to-peak values within 2 ns with the mean values within ± 3 ns. Code OSBs on C1W, C1X, and C2I signals are shown in Fig. 2b for GPS, Galileo, and BDS, respectively, and most of the satellite code OSBs have peak-to-peak values within 0.5 ns.

It is obvious that phase OSB series are less stable than code OSB series. Generally, the phase OSB of a specific satellite is a decoupling solution from wide-lane and narrow-lane UPD. According to Ge et al. (2008), wide-lane UPD series are stable within months, while narrow-lane UPDs show larger short-term variations in a day. In the estimation of phase OSBs, special alignment is made for wide-lane UPDs, making sure wide-lane UPDs of neighboring days are as consistent as possible. Narrow-lane UPDs are highly correlated with satellite clocks, thus the consistency between adjacent days is subject to clock day boundaries. Therefore, the stability of wide-lane UPD series mainly relies on code OSBs, while that of narrow-lane UPD series depends on the impacts from least-square solutions. For example, the code OSB series of E14 and E18 are not stable shown in Fig. 2, which may be caused by the highly eccentric orbit. Then, the fluctuations in the code OSBs results in the instability of the wide-lane UPD series.

Some unexpected changes in the satellite can also affect the continuity of the phase OSB series. Satellite C06 is excluded on DOY 060, due to low fixing rates, causing a re-initialization of the wide-lane UPD value on DOY 061, which is not successive to the value on DOY 059. The same re-initialization also happens for satellite C12 on DOY 067, *i.e.*, it was excluded on DOY 066 for large post-fit residuals. It is worth mentioning that satellite C12 switched from nominal attitude mode to orbit-normal attitude on DOY 066, which may cause the change of phase OSBs.

Table 3 Mean STD of the OSBs for each system

System	Mean STD for different methods (ns)	
	Code OSBs	Phase OSBs
GPS	0.11	0.30
Galileo	0.16	0.25
BDS-2	0.19	0.38
BDS-3	0.14	0.31

Note that Mean STD is the average of STD values of all the satellite OSBs without significant outliers, such as those of E14, E18, and C12 satellites.

After excluding these significant outliers, such as those of E14, E18, and C12, the average values of STD for Galileo and BDS-2/3 satellite OSBs are similar to that of GPS satellites, as shown in Table 3. Therefore, the primary reason for the phase OSB series instability is the effect of clock day boundaries, in consideration of the high correlation of OSBs and clocks, rather than system-related characteristics.
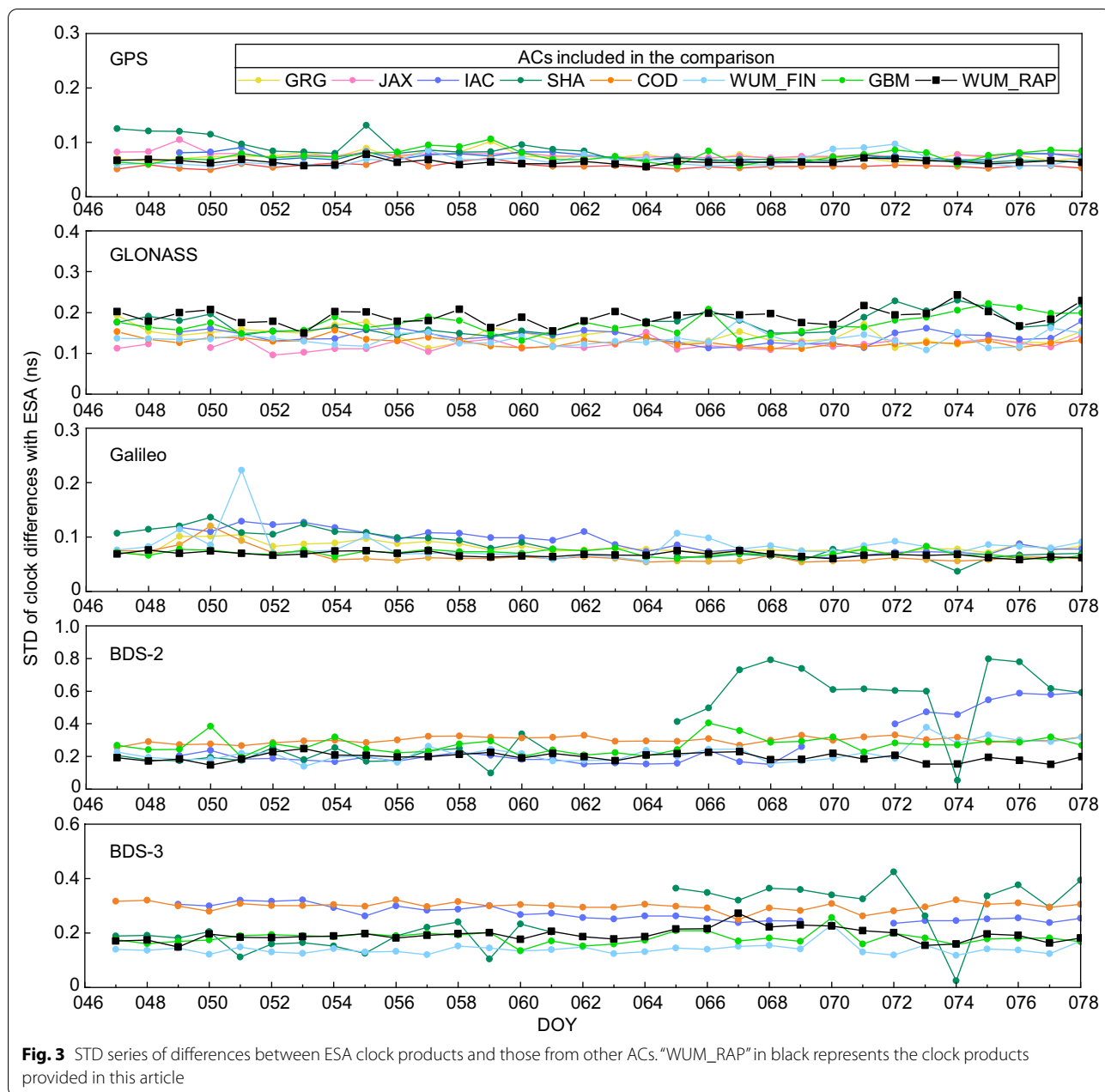
Rapid satellite clock

Differencing of clock time series is made to assess the quality of clock products, and the ESA clock product is chosen as a reference. First, the datum clock of a chosen product along with the ESA clock product is aligned to the same satellite, of which the clock offsets are subtracted from those of other satellites epoch by epoch. Since the orbit and clock parameters are highly correlated, especially in the radial component (Kouba et al., 2001), the clock comparison needs to remove the disparity of corresponding orbits. The orbits of ours and other ACs are differenced by the ESA orbits, and the radial orbit difference is stripped from the respective clock products. Then the clocks are differenced by the ESA clocks, with the STD value of their differences as the accuracy of their clocks.

Figure 3 shows that, for GPS, Galileo, BDS-2, and BDS-3, the STD series of our clock products are in a medium place among ACs. The mean STD values of our products for GPS, GLONASS, Galileo, BDS-2, and BDS-3 are 0.064 ns, 0.190 ns, 0.068 ns, 0.196 ns, and 0.193 ns, respectively. In the phase clock/bias model, the time-variable components of narrow-lane UPDs are merged into clock products, and no abnormal fluctuations are observed in GPS, Galileo, and BDS series. GLONASS products have the highest STD among ACs. The possible reason is that the more specific transmit power information is used in our earth radiation pressure model than the mean values in ERPFBOXW.F (Steigenberger et al., 2019), and later those values will be updated to the suggested values for consistency with other ACs.

Rapid satellite orbit consistency

Figure 4 shows the 3D RMS of the difference between our and other ACs' orbits with respect to that of ESA. It is worth mentioning that the RMS values represent the consistency with ESA products, thus the rank is for reference only. A 7-parameter transformation was applied. In the experimental period, our products have 3D RMS of 22.8 mm for GPS; 63.60 mm for GLONASS; 27.70 mm for Galileo; 117.87 mm for BDS-2; 86.40 mm for BDS-3. For the BDS-3 system, each AC has an RMS from each

Geng *et al. Satellite Navigation* (2022) 3:23

Page 10 of 15

Fig. 3 STD series of differences between ESA clock products and those from other ACs. "WUM_RAP" in black represents the clock products provided in this article
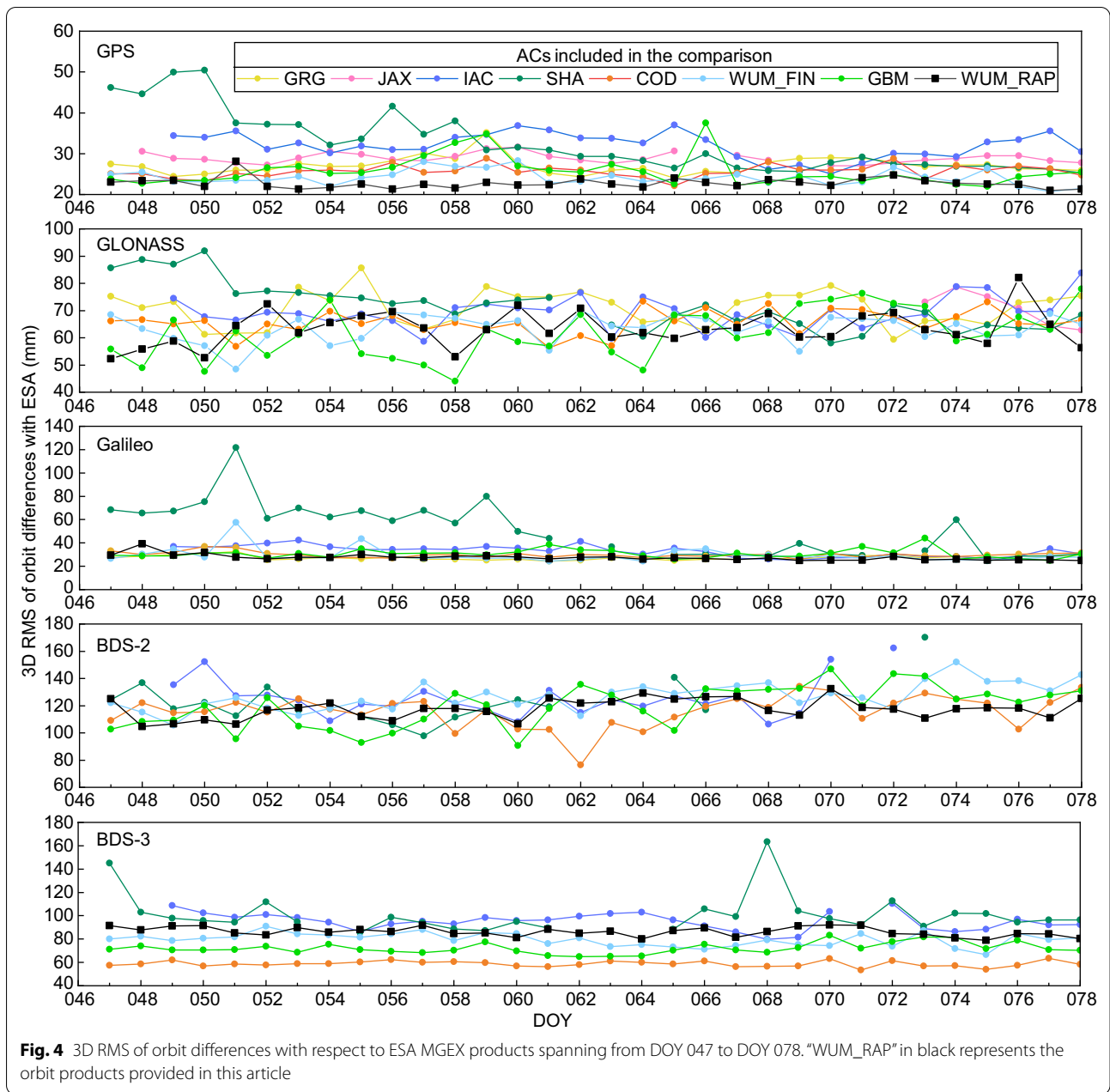
other, indicating that different models and strategies are used in their respective products. In contrast, Galileo orbits from each AC show the best consistency due to the high-quality hydrogen atomic clock and satellite metadata open to the public.

PPP-AR

The results are shown in Fig. 5, the RMS of the east, north, and up components is 0.16 cm, 0.16 cm, and 0.44 mm, respectively. The results significantly outperform the ambiguity-float results, of which the mean RMS

is 0.26 cm, 0.18 cm, and 0.56 cm in three directions. The accuracy in the east component is significantly improved after ambiguity resolution. The fixing rates are counted by all ambiguity candidates, rather than independent ambiguities. The fixing rates are listed in Table 4. The mean wide-lane fixing rate is 92.7% for GPS; 95.5% for Galileo; 92.9% for BDS-2; 92.3% for BDS-3. The narrow-lane fixing rate is the ratio of successfully fixed narrow-lane ambiguities to all the ambiguity candidates, and the detailed index is 90.2% for GPS; 93.6% for Galileo; 85.7% for BDS-2; 82.4% for BDS-3. It is worthy to mention

Fig. 4 3D RMS of orbit differences with respect to ESA MGEX products spanning from DOY 047 to DOY 078. "WUM_RAP" in black represents the orbit products provided in this article

that the BDS-2 system is regionally monitored, thus the narrow-lane fixing rates are possibly higher than those of BDS-3. The higher fixing rate of Galileo compared to GPS can be attributed to the higher accuracy of Galileo code measurements and the use of more stable atomic clocks by the Galileo satellites. The positioning results indicate that our phase OSB products can support PPP-AR well, and the millimeter-level accordance with IGS solutions implies that the strategy of products is generally consistent with IGS.

Discussion

In our work, as well as some ACs, bias products are estimated after orbit and clock products are generated. However, precise orbits are derived based on a network solution utilizing double-difference ambiguity resolution, which is slightly different from the between-satellite single-difference AR used in ionosphere-free PPP-AR. Although two AR methods are mathematically the same, many studies indicate that they practically lead to different results. Ruan et al. (2018) found that GPS orbit precision was slightly improved by fixing the between-satellite

Fig. 5 RMS of position difference with IGS weekly solutions. One point represents a solution at a station on a day
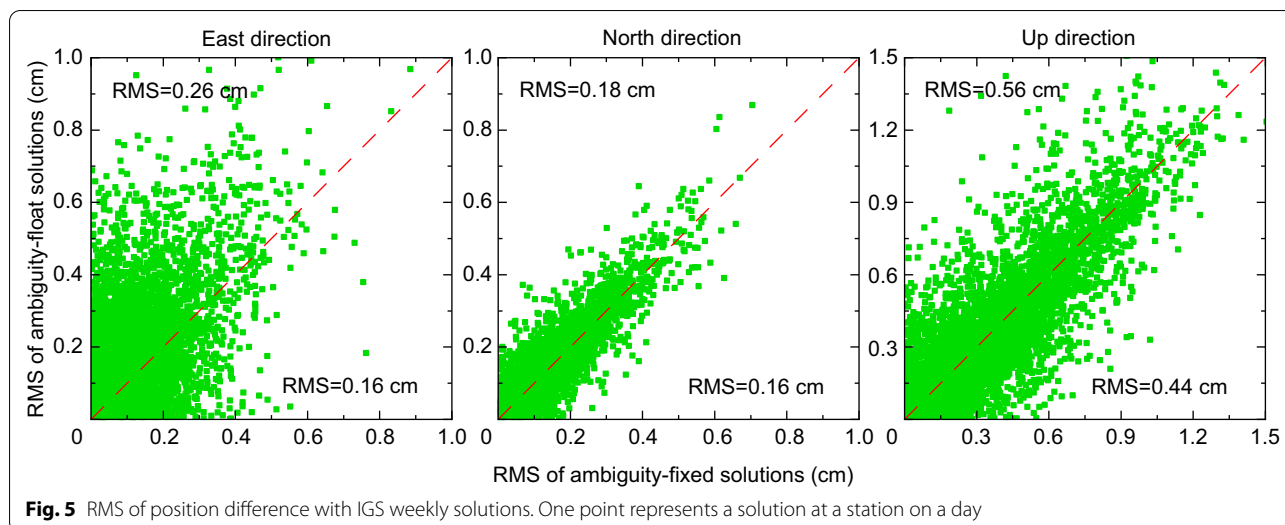
single-difference ambiguities instead of double-difference ambiguities, but the reason was not discussed. Geng et al. (2021) compared two methods in a massive network solution, finding that the double-difference AR are contaminated by about 0.8% "redundant" ambiguities, and thus the solutions are inferior to those with the between-satellite single-difference AR. Considering the difference between the two AR methods, the orbit parameters should be updated with the between-satellite single-difference AR to keep consistent with bias products.

To evaluate the influence of different AR strategies on satellite orbit, we compare the orbit precision of the between-satellite single-difference AR, the double-difference AR, and the ambiguity-float solutions. GPS, Galileo, and BDS-3 MEO systems are included in our verification, and POD is conducted apart to avoid propagation of errors. BDS-2 and BDS-3 IGSO satellites are excluded because their AR results are not reliable. The Orbit Boundary Discontinuities (OBDs) are computed to evaluate the internal consistency of orbits. To avoid coincidence, we use a short prediction of 10 epochs with an interval of 30 s instead of one boundary epoch. In the processing, orbits cannot reach their highest theoretical precision suffering from bad-quality observations and

baselines, and thus gross errors are detected with the 3-sigma principle and removed in our results.

As illustrated in Fig. 6, the between-satellite single-difference AR solutions have the smallest RMS of OBDs for all satellites involved. Ambiguity-float BDS-3 orbits show the worst precision because the satellites manufactured by Shanghai Engineering Center for Microsatellites (SECM) have more noise in pseudorange signals (Zhang et al., 2019). More detailed statistics are listed in Table 5. Comparing the between-satellite single-difference AR solutions with the double-difference AR solutions, GPS, Galileo, and BDS-3 orbit accuracies are improved by 14%, 17%, and 24%, respectively. The results indicate that the between-satellite single-difference AR can also benefit POD processing, which may facilitate the shift and development of POD from traditional double-difference AR to the between-satellite single-difference AR.
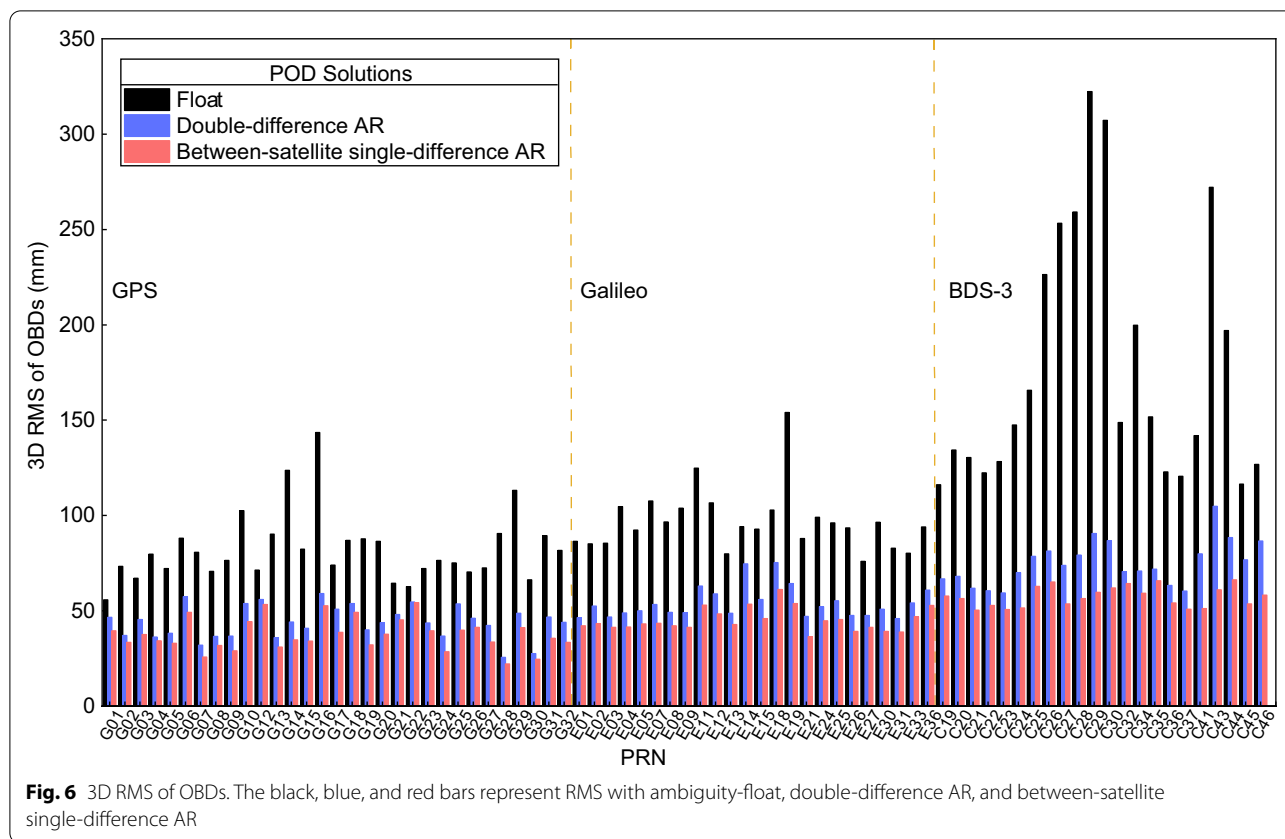
Conclusion

In this article, the observable-specific phase bias products at Wuhan Multi-GNSS Experiment Analysis Center are introduced, including the models and processing strategies. The associated orbit and clock products are also introduced, and the consistency is portrayed in comparison with the products from other AC. Meanwhile, the impact of the between-satellite single-difference ambiguity AR with our phase bias products on precise orbit determination is discussed. We validated our products by PPP-AR and found that our products can lead to high-accuracy positioning results.

Satellite clock and phase bias products are highly correlated. To further improve the consistency, we provide

Table 4 Mean fixing rates of PPP-AR results

System	Wide-lane ambiguity (%)	Narrow-lane ambiguity (%)
GPS	92.71	90.16
Galileo	95.54	93.55
BDS-2	92.92	85.67
BDS-3	92.26	82.40

Fig. 6 3D RMS of OBDs. The black, blue, and red bars represent RMS with ambiguity-float, double-difference AR, and between-satellite single-difference AR

Table 5 RMS of GPS, Galileo, BDS-3 MEO OBDs in each direction (mm)

Mode of solutions	RMS of 3D	RMS in along-track direction	RMS in cross-track direction	RMS in radial direction
GPS Float	84.2	66.4	42.5	28.2
GPS Double-difference AR	44.7	30.0	23.3	22.4
GPS Between-satellite SD AR	38.3	24.6	20.2	20.8
Galileo Float	98.0	78.4	44.8	37.5
Galileo Double-difference AR	54.7	36.3	25.8	30.4
Galileo Between-satellite SD AR	45.4	27.1	22.7	27.8
BDS-3 Float	189.1	166.4	70.2	55.3
BDS-3 Double-difference AR	75.9	55.7	33.5	39.1
BDS-3 Between-satellite SD AR	57.7	36.9	28.8	33.2

complete products including precise ephemeris, precise clocks, attitude quaternion, and ERP. Our processing follows a routine of IGS rapid products and meet the requirements of IGS PPP-AR working groups, and all these products are uploaded with a latency less than 16 h. Currently, we have provided multi-GNSS products traced back to 2020, and these products are updated on the FTP website of WHU.

Our phase bias products are in the OSB framework recommended by the IGS. The OSB time series within a month have peak-to-peak values within 2 ns, with the mean values within ± 3 ns. For most satellites, the fluctuation of the OSB series is caused by a day-by-day processing strategy. The associated orbits and clocks are in comparison with existing MGEX products, with ESA products as reference. Our GPS orbit products have the

best consistency with ESA, while Galileo and BDS products rank in a medium place among ACs.

We validate our products by PPP-AR with the open-source software PRIDE PPP-AR. The multi-GNSS PPP-AR solutions can reach an accuracy of 0.16 cm, 0.16 cm, and 0.44 cm in the east, north, and up directions respectively. The wide-lane fixing rates of the multi-GNSS systems are all above 90%, while the narrow-lane fixing rates above 80%. The results show that our phase products have good accuracy, leading to successful ambiguity resolution.

Finally, we propose that an update of orbit with well-estimated phase OSB products is necessary. On the one hand, an update ensures the consistency of OSB and orbit products; on the other hand, the between-satellite single-difference AR has advantages proved in previous studies. This step can remarkably increase the inner precision of orbits. In our experiment, the RMS of OBDs of GPS, Galileo, and BDS-3 orbit is reduced by 14%, 17%, and 24%, respectively.

Author contributions
JG led the project; QZ and GL derived all technical analysis; QZ carried out all computation and software development; QZ drafted the article; JG, GL, JL and DL revised the article. All authors read and approved the final manuscript.

Availability of data and materials
The datasets used and/or analyzed during the current study are available from the corresponding author on reasonable request.

Declaration

Competing interests
The authors declare that they have no competing interests.

Author details
[1]GNSS Research Center, Wuhan University, 129 Luoyu Road, Wuhan 430079, China. [2]Hubei Luojia Laboratory, Wuhan University, 129 Luoyu Road, Wuhan 430079, China. [3]Natural Resources Satellite Remote Sensing Application Center, 242 Zhonghuabei Road, Guiyang 550004, China.

References

Banville, S., Geng, J., Loyer, S., et al. (2020). On the interoperability of IGS products for precise point positioning with ambiguity resolution. *Journal of Geodesy, 94*(1), 1–15.

Beutler, G., Moore, A. W., & Mueller, I. I. (2009). The international global navigation satellite systems service (IGS): Development and achievements. *Journal of Geodesy, 83*(3), 297–307.

Boehm, J., Heinkelmann, R., & Schuh, H. (2007). Short Note: A global model of pressure and temperature for geodetic applications. *Journal of Geodesy, 81*(10), 679–683.

Chen, J., Zhang, Y., Zhou, X., Pei, X., Wang, J., & Wu, B. (2014). GNSS clock corrections densification at SHAO: From 5 min to 30 s. *Science China Physics, Mechanics and Astronomy, 57*(1), 166–175.

Collins, P., Bisnath, S., Lahaye, F., et al. (2010). Undifferenced GPS ambiguity resolution using the decoupled clock model and ambiguity datum fixing. *Navigation, 57*(2), 123–135.

Dilssner, F. (2010). GPS IIF-1 satellite antenna phase center and attitude modeling. *Inside GNSS, 5*(6), 59–64.

EGSC. (2017). Galileo satellite metadata. European GNSS Service Centre, https://www.gsc-europa.eu/support-to-developers/galileo-satellite-metadata.

Ge, M., Gendt, G., Rothacher, M. A., Shi, C., & Liu, J. (2008). Resolution of GPS carrier-phase ambiguities in precise point positioning (PPP) with daily observations. *Journal of Geodesy, 82*(7), 389–399.

Geng, J., Chen, X., Pan, Y., Mao, S., Li, C., Zhou, J., & Zhang, K. (2019a). PRIDE PPP-AR: An open-source software for GPS PPP ambiguity resolution. *GPS Solutions, 23*(4), 1–10.

Geng, J., Chen, X., Pan, Y., & Zhao, Q. (2019b). A modified phase clock/bias model to improve PPP ambiguity resolution at Wuhan University. *Journal of Geodesy, 93*(10), 2053–2067.

Geng, J., Wen, Q., Zhang, Q., Li, G., & Zhang, K. (2022). GNSS observable-specific phase biases for all-frequency PPP ambiguity resolution. *Journal of Geodesy, 96*(2), 1–18.

Geng, J., & Mao, S. (2021). Massive GNSS network analysis without baselines: Undifferenced ambiguity resolution. *Journal of Geophysical Research: Solid Earth,* 126(10), e2020JB021558. https://doi.org/10.1029/2020JB021558.

Guo, J., Xu, X., Zhao, Q., & Liu, J. (2016). Precise orbit determination for quad-constellation satellites at Wuhan University: Strategy, result validation, and comparison. *Journal of Geodesy, 90*(2), 143–159.

Jiao, G., Song, S., & Jiao, W. (2019). Improving BDS-2 and BDS-3 joint precise point positioning with time delay bias estimation. *Measurement Science and Technology, 31*(2), 025001.

Kouba, J. (2009). A simplified yaw-attitude model for eclipsing GPS satellites. *GPS Solutions, 13*(1), 1–12.

Kouba, J., & Springer, T. (2001). IGS station and satellite clock combination. *GPS Solutions, 4*(4), 31–36.

Kouba, J. (2013). Noon turns for deep eclipsing Block IIF GPS satellites. A note prepared for IGS ACs, IGS-ACS-930 Mail.

Laurichesse, D. (2015). Carrier-phase ambiguity resolution: Handling the biases for improved triple-frequency PPP convergence. *GPS World, 26*(4), 49–54.

Laurichesse, D., Mercier, F., Berthias, J. P., Broca, P., & Cerri, L. (2009). Integer ambiguity resolution on undifferenced GPS phase measurements and its application to PPP and satellite precise orbit determination. *Navigation, 56*(2), 135–149.

Lin, X., Lin, B., Liu, Y., Xiong, S., & Bai, T. (2018). Satellite geometry and attitude mode of BeiDou-3 MEO satellites developed by SECM. In *Proceedings of the 31th international technical meeting of the satellite division of the institute of navigation (ION GNSS+ 2018)*, Miami, Florida, 1268–1289.

Liu, T., & Zhang, B. (2021). Estimation of code observation-specific biases (OSBs) for the modernized multi-frequency and multi-GNSS signals: An undifferenced and uncombined approach. *Journal of Geodesy, 95*(8), 1–20.

Lou, Y., Liu, Y., Shi, C., Yao, X., & Zheng, F. (2014). Precise orbit determination of BeiDou constellation based on BETS and MGEX network. *Scientific Reports, 4*(1), 1–10.

Loyer, S., Banville, S., Geng, J., & Strasser, S. (2021). Exchanging satellite attitude quaternions for improved GNSS data processing consistency. *Advances in Space Research, 68*(6), 2441–2452.

Loyer, S., Banville, S., Perosanz, F., & Mercier, F. (2017). Disseminating GNSS satellite attitude for improved clock correction consistency. In *Proceedings of the 2017 IGS Workshop*, Paris, France, 3–7.

Montenbruck, O., Steigenberger, P., Khachikyan, R., Weber, G., Langley, R., Mervart, L., & Hugentobler, U. (2014). IGS-MGEX: Preparing the ground for multi-constellation GNSS science. *Inside GNSS, 9*(1), 42–49.

Ruan, R., Wei, Z., & Feng, L. (2018). Satellite clock estimation with between satellite single difference phase ambiguity fixing. *Acta Geodaeticaet Cartographica Sinica, 47*(7), 916–923.

Schaer, S., Villiger, A., Arnold, D., Dach, R., Prange, L., & Jäggi, A. (2021). The CODE ambiguity-fixed clock and phase bias analysis products: Generation, properties, and performance. *Journal of Geodesy, 95*(7), 1–25.

Schaer, S. (2016a). Bias-SINEX format and implications for IGS bias products. In *IGS Workshop* (pp. 8–12). Sydney, Australia, February.

Schaer, S. (2016b). SINEX BIAS-solution (software/technique) INdependent EXchange Format for GNSS BIASes Version 1.00. In IGS workshop on GNSS biases (pp. 1–37). Bern, Switzerland, February.

Spiridonov, E. A., & Vinogradova, O. Y. (2020). Oceanic Tide Model FES2014b: Comparison with Gravity Measurements. *Izvestiya, Atmospheric and Oceanic Physics*, *56*(11), 1432–1446.

Springer, T. A., Beutler, G., & Rothacher, M. (1999). A new solar radiation pressure model for GPS satellites. *GPS Solutions, 2*(3), 50–62.

Steigenberger, P., Thoelert, S., & Montenbruck, O. (2020). GPS III Vespucci: Results of half a year in orbit. *Advances in Space Research, 66*(12), 2773–2785.

Steigenberger, P., Thoelert, S., & Montenbruck, O. (2019). GPS and GLONASS satellite transmit power: Update for igs repro3. http://acc.igs.org/repro3/TX_Power_20190711.pdf.

Strasser, S., Mayer-Gürr, T., & Zehentner, N. (2019). Processing of GNSS constellations and ground station networks using the raw observation approach. *Journal of Geodesy, 93*(7), 1045–1057.

Wang, C., Guo, J., Zhao, Q., & Liu, J. (2018a). Yaw attitude modeling for BeiDou I06 and BeiDou-3 satellites. *GPS Solutions, 22*(4), 1–10.

Wang, C., Guo, J., Zhao, Q., & Liu, J. (2018b). Solar radiation pressure models for BeiDou-3 I2-S satellite: comparison and augmentation. *Remote Sensing., 10*(1), 118.

Xia, F., Ye, S., Chen, D., & Jiang, N. (2019). Observation of BDS-2 IGSO/MEOs yaw-attitude behavior during eclipse seasons. *GPS Solutions, 23*(3), 1–16.

Yan, X., Liu, C., Huang, G., et al. (2019). A priori solar radiation pressure model for BeiDou-3 MEO satellites. *Remote Sensing, 11*(13), 1605.

Zhang, Q., & Zhao, Q. L. (2020). Global ionosphere mapping and differential code bias estimation during low and high solar activity periods with GIMAS software. *Remote Sensing, 10*(5), 705.

Zhang, B., Jia, X., Sun, F., Xiao, K., & Dai, H. (2019). Performance of BeiDou-3 satellites: Signal quality analysis and precise orbit determination. *Advances in Space Research, 64*(3), 687–695.

Publisher's Note